Journal of Geophysical Research: Space Physics

RESEARCH ARTICLE
10.1002/2017JA024562

Key Points:
- The dayside detached auroras caused by the solar wind pressure enhancement were observed in both hemispheres
- The detached auroras were dominated by hot ions/protons, with energies ranging from 20 keV to more than 240 keV
- The particles in the detached auroras were scattered into the loss cone by EMIC waves and mapped to the vicinity of plasmapause

Correspondence to:
X. Luan,
luanxl@ustc.edu.cn

Citation:
Zhou, S., Luan, X., Søraas, F., Østgaard, N., & Raita, T. (2018). The detached auroras induced by the solar wind pressure enhancement in both hemispheres from imaging and in situ particle observations. *Journal of Geophysical Research: Space Physics*, *123*, 3170–3182. https://doi.org/10.1002/2017JA024562

Received 7 JUL 2017
Accepted 28 MAR 2018
Accepted article online 6 APR 2018
Published online 21 APR 2018

The Detached Auroras Induced by the Solar Wind Pressure Enhancement in Both Hemispheres From Imaging and In Situ Particle Observations

Su Zhou[1,2], Xiaoli Luan[1], Finn Søraas[2], Nikolai Østgaard[2], and Tero Raita[3]

[1]CAS Key Laboratory of Geospace Environment, School of Earth and Space Sciences, University of Science and Technology of China, Hefei, China, [2]Birkeland Centre for Space Science, University of Bergen, Bergen, Norway, [3]Sodankylä Geophysical Observatory, University of Oulu, Oulu, Finland

Abstract This paper presents simultaneous detached proton auroras that appeared in both hemispheres at 11:06 UT, 08 March 2012, just 2 min after a sudden solar wind pressure enhancement (~11:04 UT) hit the Earth. They were observed under northward interplanetary magnetic field Bz condition and during the recovery phase of a moderate geomagnetic storm. In the Northern Hemisphere, Defense Meteorological Satellite Program/Special Sensor Ultraviolet Spectrographic Imager observed that the detached arc occurred within 60°–65° magnetic latitude and covered a few magnetic local time (MLT) hours ranging from 0530 to 0830 MLT with a possible extension toward noon. At the same time (11:06 UT), Polar Orbiting Environment Satellites 19 detected a detached proton aurora around 1300 MLT in the Southern Hemisphere, centering ~62° magnetic latitude, which was at the same latitudes as the northern detached arc. This southern aurora was most probably a part of a dayside detached arc that was conjugate to the northern one. In situ particle observations indicated that the detached auroras were dominated by protons/ions with energies ranging from around 20 keV to several hundreds of keV, without obvious electron precipitations. These detached arcs persisted for less than 6 min, consistent with the impact from pressure enhancement and the observed electromagnetic ion cyclotron (EMIC) waves. It is suggested that the increasing solar wind pressure pushed the hot ions in the ring current closer to Earth where the steep gradient of cold plasma favored EMIC wave growth. By losing energy to EMIC waves the energetic protons (>20 keV) were scattered into the loss cone and produced the observed detached proton auroras.

1. Introduction

The auroral oval is the primary region, where energetic electrons and ions precipitations take place. In addition, there exist some optical features separated from the auroral oval (Frey, 2007; Immel et al., 2002). They have received a lot of interests since first reported by Moshupi et al. (1977) and Anger et al. (1978) using ISIS-2 observations. Detached auroras usually occur at the subauroral latitudes and have different names such as "detached arc" (Burch et al., 2002), "subauroral proton flash" (Hubert et al., 2003), "dayside detached auroras" (Zhang et al., 2002), and "corotating detached patch" (Frey, 2007). Detached auroras could be caused by different physical mechanisms. For example, the change of interplanetary magnetic field (IMF) By and Bz cause the auroral arc separated from the auroral oval in the afternoon sector (Immel et al., 2002). The present study will report a detached aurora induced by a solar wind dynamic pressure enhancement.

The solar wind pressure increase might lead to the persistent global proton aurora (Laundal & Østgaard, 2008) and trigger the proton precipitations, which are separated from the equatorward edge of the auroral oval (Fuselier et al., 2004; Hubert et al., 2003, 2005; Søraas et al., 2013; Yahnina et al., 2008; Zhang et al., 2002, 2008). In general, the detached auroras caused by the solar wind pressure pulses (shocks) have short durations less than 10 min (Fuselier et al., 2004; Hubert et al., 2003, 2005; Zhang et al., 2002). These detached auroras form preferentially in the noon sector (Fuselier et al., 2004; Hubert et al., 2003; Zhang et al., 2004; Zhou & Tsurutani, 1999), and they can also be seen in the nighttime sector (Zhang et al., 2008). Søraas et al. (2013) showed a long detached arc in the early morning sector associated with a solar wind pressure enhancement. In their study the solar wind pressure increased gradually and the detached arc persisted for about 2 hr, which is different from most shock-induced detached auroras. Zhang et al. (2002) used Defense Meteorological Satellite Program (DMSP) in situ observations to show that the shock-induced detached aurora was composed of protons with energies of ~10 keV with obvious electron precipitations.

These protons from the ring current are the dominant energy source for the detached aurora caused by the pressure enhancement. Further, they suggested the proton energies for the detached aurora might be higher than 10 keV, since the DMSP cannot observe particles with energies above 30 keV. Hubert et al. (2005) studied the shock-induced detached arcs statistically, which they called dayside subauroral proton flashes, showing that their lifetime is not governed by the solar wind properties. In particular, they showed that the proton auroral power of these arcs is directly related to the dynamic pressure increase, which characterizes the solar wind discontinuity.

Wave-particle interaction was suggested to be the dominant mechanism for the detached aurora. The perpendicular kinetic energy of electrons and ions will increase when the magnetosphere is compressed by sudden solar wind pressure enhancement, as the first adiabatic invariant is conserved (Anderson & Hamilton, 1993; Fuselier et al., 2004; Usanova et al., 2010; Zhang et al., 2008; Zhou & Tsurutani, 1999). The electromagnetic ion cyclotron (EMIC) waves can be generated by temperature anisotropy, scattering the energetic ions into the loss cone (Anderson & Hamilton, 1993; Fuselier et al., 2004; Søraas et al., 2013; Zhang et al., 2008). Zhang et al. (2008) observed EMIC waves associated with the shock-induced aurora, by using the data of Polar satellite. Fuselier et al. (2004) discussed the role of the growth rate of EMIC waves, which lacked support from direct wave observations. In the present study, we will present detached auroras caused simultaneously by the solar wind pressure enhancement in conjugate latitudes of both hemispheres. Combining observations from DMSP and National Oceanic and Atmospheric Administration (NOAA) Polar Orbiting Environment Satellites (POES), we determined the particle energies for the detached auroras. NOAA POES can measure the protons and electrons with energies above 30 keV. The EMIC wave data were collected during the periods when the detached auroras occurred, using magnetic data in three ground stations in Finland.

This paper is organized as follows. In section 2, we will briefly introduce the instruments and data used in the present study. Then, in section 3, we will display the results of the detached auroras, using data from ultraviolet imagers and the simultaneous in situ particle observations from the DMSP and NOAA POES. In section 4, we will discuss the possible mechanisms related to this detached aurora. The summary and conclusions are given in the last section.

2. Data

The DMSP is a Sun-synchronous, near-polar orbit satellite, operating at an altitude of ~830 km. It has an orbital period of 101 min. The Special Sensor Ultraviolet Spectrographic Imager (SSUSI) on board DMSP satellite is a remote sensing instrument which records auroral ultraviolet emissions in five different wavelengths: H (Lyman α, 121.6 nm), OI (130.4 nm), OI (135.6 nm), N_2 Lyman-Birge-Hopfield Short (LBHS, 140.0–160.0 nm) and Long (LBHL, 160.0–180.0 nm) band emissions (Paxton et al., 2002; Sotirelis et al., 2013). The LBHS could be reduced due to O_2 Schumann-Runge absorption, but there is less significant absorption in LBHL band (Germany et al., 1990). The SSUSI reaches its highest resolution of ~7 km at nadir, allowing us to easily capture auroral structures. The SSUSI consists of a cross-tracking mirror, and each obtained image covers approximately one third to approximately one half of the auroral oval. The first SSUSI was on board the DMSP F16 satellite launched on 18 October 2003. DMSP F17 and F18 were launched respectively in November 2006 and October 2009. Another instrument on board the DMSP satellite, the Special Sensor J (SSJ), is designed to monitor the energy and flux of both electrons and ions. The instrument looks toward the satellite zenith and detects the particles with a kinetic energy ranging from 30 eV to 30 keV in 19 logarithmically spaced energy channels (Newell, 2000).

In addition to the DMPS satellites, we used data from NOAA POES satellites, which fly in Sun-synchronous orbits at an altitude of ~830 km with an orbital period of 102 min. The Medium Energy Proton and Electron Detector (MEPED), on board the POES, consists of two directional electron telescopes and two directional proton telescopes. One telescope points radially upward, called the 0° detector, and the other telescope is called the 90° detector perpendicular to the first one. The MEPED views protons and electrons above 30 keV in the vertical and horizontal directions with a time resolution of 2 s. The field of view of both detectors is 30°. At high latitudes, the 0° detector monitors the particles flowing down in the loss cone along the magnetic field, while the 90° detector is oriented perpendicularly to that direction. The POES are also equipped with a Total Energy Detector (TED) instrument, using two telescopes to measure protons and

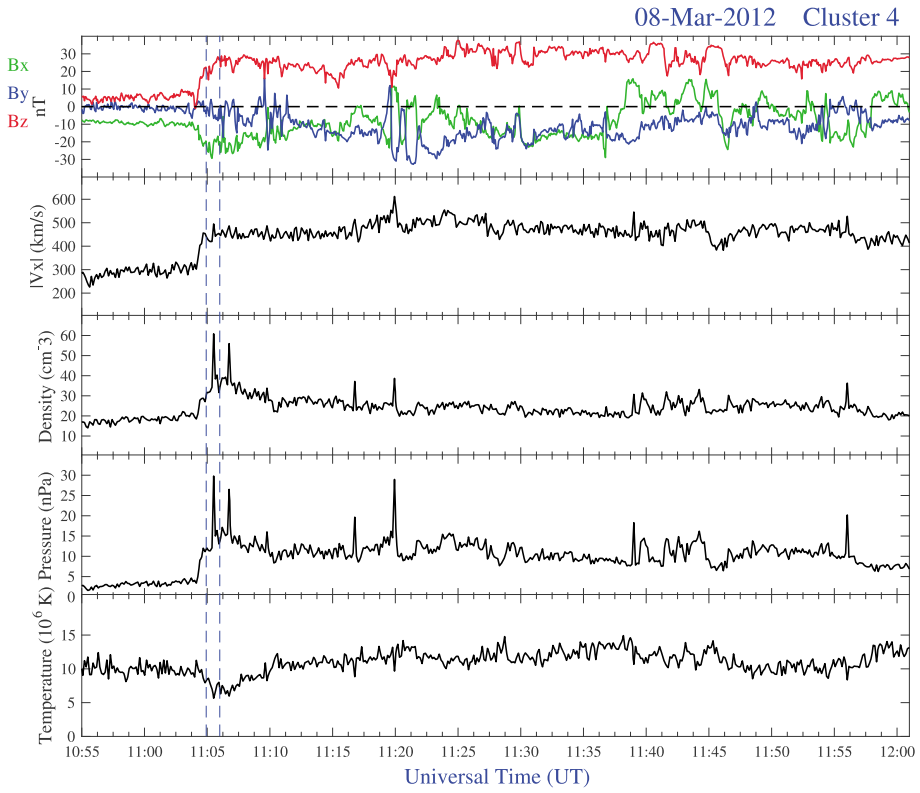

Figure 1. The interplanetary magnetic field (IMF) in GSM coordinate and solar wind plasma conditions between 10:55 and 12:01 UT on 8 March 2012 from Cluster observation. From top to bottom are components of IMF, *x* component of solar wind speed, proton density, plasma dynamic pressure, and plasma temperature. The IMF and solar wind plasma data have been shifted to the location of magnetopause. The two dashed lines note 11:05 and 11:06 UT, respectively.

electrons: one points the zenith direction and the other one in a 30° off the first one. TED measures both protons and electrons from 254 eV to 20 keV in five energy bands, with a time resolution of 8 s. The total energy input due to particles with energy below 20 keV is evaluated from the TED measurement. For a full description of the instrumentation on board the POES satellite; see Evans and Greer (2000). The MEPED data used in this study are calibrated using the method by Sandanger et al. (2015).

We also use the Finnish pulsation magnetometers to investigate the horizontal magnetic pulsations in the present work. They are operated by the Sodankylä Geophysical Observatory, University of Oulu. Each pulsation magnetometer has two horizontal coils, with one oriented in the H direction and the other normal to it. The magnetometers sample data with a frequency of 40 Hz.

The solar wind plasma and IMF conditions are monitored by the Cluster satellite, which has a nearly 90° inclination and an orbital period of 57 hr. The perigee and apogee of Cluster are located around 4 R_E and 20 R_E in distance, respectively. On 8 March 2012, when a detached auroral arc was observed by the DMSP/SSUSI at around 11:06 UT, the Cluster was favorably located near $X = 16.3$ R_E, $Y = 2.7$ R_E, $Z = -12.4$ R_E in GSM coordinate. At that time Cluster was very close to the magnetopause, providing more appropriate solar wind data than Wind satellite, which was located ~208 R_E away from the Earth. These instruments and data described above will be used to investigate a detached proton aurora happened on 8 March 2012.

3. Results

3.1. DMSP Observations of the Detached Aurora

On 8 March 2012, an interplanetary shock associated with a coronal mass ejection hit the Earth's magnetosphere around 11:04 UT. Figure 1 gives the solar wind plasma and IMF conditions during the period from 10:55 UT to 12:00 UT, which has been shifted to the magnetopause. The Cluster might be inside the

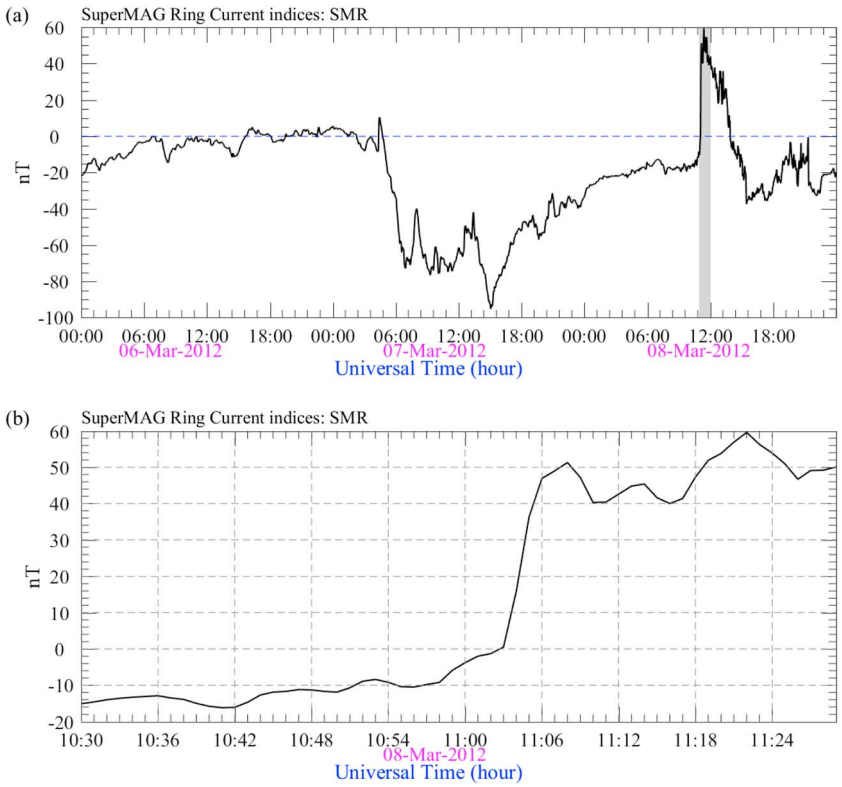

Figure 2. (a) SuperMag ring current indices (SMR) from 6 to 8 March 2012. The dark area corresponds to the period of interest, from 10:55 to 12:00 UT. (b) SMR indices between 10:30 and 11:30 UT on 8 March 2012.

magnetosheath as the solar wind plasma temperature was pretty high and the corresponding sonic Mach number was less than 1. The average location of magnetopause is estimated to be 10 R_E from the center of the Earth (Shue et al., 1997). When the interplanetary shock (IP) occurred, the Cluster was located near $X = 16.3\ R_E$, $Y = 2.7\ R_E$, $Z = -12.4\ R_E$ in GSM coordinate. Solar wind velocity was ~450 km/s. Earth's radius is 6,371 km. Thus, the approximate travel time to the magnetopause was estimated to be ~1.5 min. Looking closely at the blue dotted line in Figure 1, the solar wind dynamic pressure increased sharply from 3 to ~12 nPa within ~1 min (solar wind dynamic ramp), which started at ~11:04 and it followed by two pressure pulses with peaks of 30 nPa shortly after ~11:05 UT and 25 nPa shortly after ~11:06 UT. The pressure ramp starting at ~11:04 UT might trigger a detached ion aurora, which will be discussed later. The IMF Bz was directed northward (~20 nT). The Bx component was about −30 nT, and the By component was nearly zero.

Figure 2a gives details of the SuperMag Ring current indices (SMR). The dark area notes the period of interest as shown in Figure 1. Here we can see the solar wind dynamic pressure enhancement took place in the recovery phase of a moderate storm of −90 nT, starting the day before. Thus, the solar wind dynamic pressure enhancement occurred when the magnetosphere was slightly inflated by hot ring current protons. Consequently, the inner magnetosphere contained a fair number of ring current ions, which can be expected to be mostly protons. Figure 2b shows the SMR indices during 10:30 and 11:30 UT on 8 March 2012. As seen from the Figure 2b, the SMR jumped from 0 to 50 nT during 11:03 and 11:06 UT. That was the same time as the pressure started to rise suddenly.

When the interplanetary shock compressed the magnetopause, the DMSP F18, F16, and F17 satellites flew over the Northern Hemisphere one after the other. Figure 3 gives the LBHS (a–c) and LBHL (d–f) images from DMSP F18/SSUSI (a and d), F16/SSUSI (b and e), and F17/SSUSI (c and f), respectively. Figure 3b exhibits a detached aurora that occurred at the dawnside and was separated by ~5° magnetic latitude (MLAT) from the equatorward edge of the northern auroral oval. This detached aurora was captured by the DMSP F16/SSUSI at 11:06 UT, just 2 min after the enhanced pressure struck the Earth (11:04 UT). It expanded across a few degrees in MLAT within 60°–65° and extended from 0530 to 0830 magnetic local time (MLT). It could

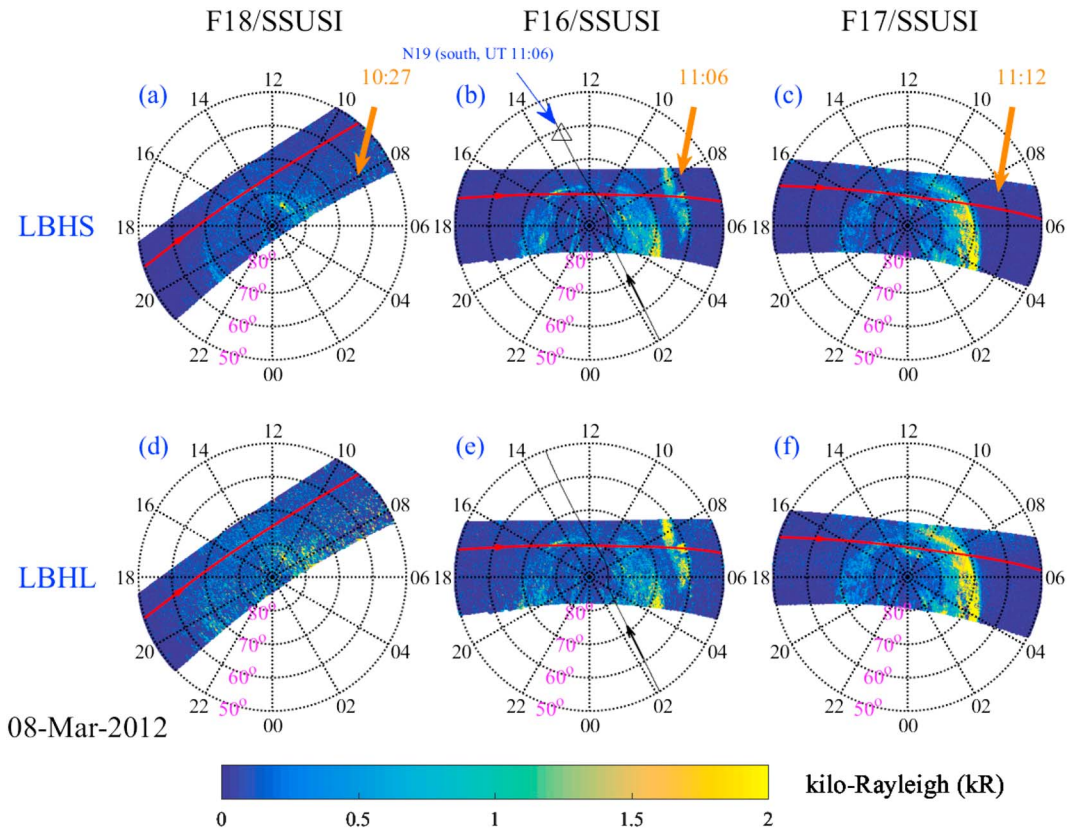

Figure 3. A series of northern hemisphere auroras observed by F18/Special Sensor Ultraviolet Spectrographic Imager (SSUSI) (a and d), F16/SSUSI (b and e) and F17/SSUSI (e and f) on 8 March 2012. These images are plotted in magnetic coordinate with magnetic latitude of 50°, 60°, 70° and 80° marked. The top (a–c) and bottom (d–f) three images show the Lyman-Birge-Hopfield Short (LBHS) (140–160 nm) and Lyman-Birge-Hopfield Long (LBHL) (160–180 nm), respectively. An auroral arc, separated from the auroral oval and indicated by a yellow arrow, can be seen from (b) and (e). The red and black lines show the footprints of the Defense Meteorological Satellite Program and Polar Orbiting Environment Satellites 19 (POES 19), the moving directions being indicated by the red and black arrows, respectively. The universal time when the DMSP satellites scan the dayside is indicated above the arrows. The triangle shown in panel b indicates the conjugate location of National Oceanic and Atmospheric Administration POES 19.

have a longer extension in MLT because its dayside part toward noon was outside the field of view of SSUSI. After a few minutes, Figure 3c shows that at ~11:12 UT, the detached arc was absent. In addition, the detached arc did not occur around 10:27 UT, when the F18/SSUSI (Figure 3a) flew across the same location where the detached arc occurred. Thus, the detached arc was expected to occur after 10:27 UT and disappear before 11:12 UT. There was a good association between the occurrence time of the observed detached arc and solar wind dynamic pressure enhancement, similar to those reported by previous studies (Fuselier et al., 2004; Hubert et al., 2003; Zhang et al., 2002). Since the SMR increase starts at ~11:03–11:04 UT which points to a relation with the solar wind pressure enhancement at ~11:04 UT, this pressure enhancement is expected to trigger the detached arc, and the two pressure pulses after 11:05 UT both contribute to the occurrence of the detached arc. The LBHL (Figure 3e) luminosity from the detached arc is stronger than the LBHS (Figure 3b). This indicates that the auroral emissions are strongly absorbed by O_2 and therefore originate at relatively low altitude, so that the detached arc is likely produced by energetic particles. However, it is impossible to determine the kind of particles producing the detached arc, using the FUV LBH images only.

Figure 4 displays the particle observations obtained along the DMSP F16 track shown in Figure 3. The precipitating particles responsible for the detached arc were clearly observed around 11:06 UT and centered at ~63° MLAT, in line with the result of ultraviolet images (Figures 3b and 3e). As seen from Figure 4, the detached arc was solely produced by ions, without any electron precipitations. Especially, the detected

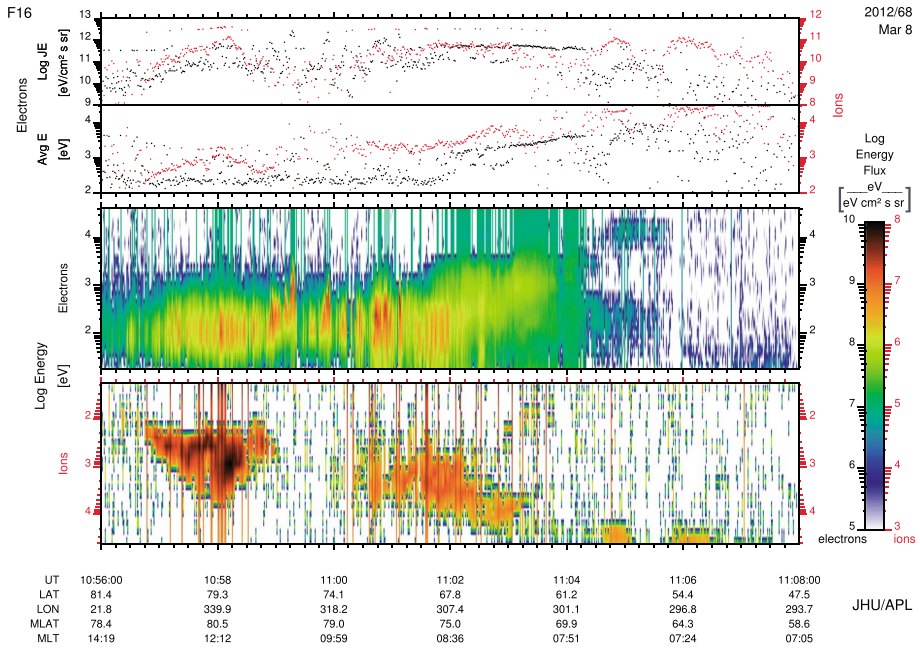

Figure 4. The Defense Meteorological Satellite Program (DMSP) F16 in situ observations coincident with the images of Figures 1b and 1e, illustrating the particle data detected by the Special Sensor J instrument on board the DMSP F16 satellite. The different panels show, from top to bottom, the integral energy flux, average energy, and differential energy flux for electrons and ions. The *y* axis are logarithmic. MLAT = magnetic latitude; MLT = magnetic local time; JPU = Johns Hopkins University; APL = Applied Physics Laboratory.

particles producing the detached arc were predominantly high-energy protons above ~20 keV. But they probably exceeded 30 keV, beyond the upper limit of the DMSP/SSJ instrument.

As shown above, the DMSP F16/SSUSI observed the detached arc at 11:06 UT on 8 March 2012 in the Northern Hemisphere. Nearly at the same time, the DMSP F18/SSUSI flew over the Southern Hemisphere and caught the dawnside auroral oval. Figure 5a shows the F18/SSUSI picture on 8 March 2012 in the Southern Hemisphere. The coincident in situ observation is given in Figure 5b. Around 11:05 UT, the southern dawnside auroral oval was monitored by both the SSUSI and SSJ instruments. It is just 1 min after the sudden pressure enhancement hit the Earth. However, Figure 5 showed that no detached aurora was observed in the southern dawnside around 63° MLAT, which is the magnetically conjugate location to the northern dawnside where the detached arc was seen. It is possible that the detached arc occurred slightly after 11:05 UT. In addition, the arc disappeared at 11:12 UT (Figure 3c). Thus, the detached arc may be lasted for less than 6 min, which is consistent with the duration of shock-induced detached arc reported by previous studies (Fuselier et al., 2004; Hubert et al., 2003; Zhang et al., 2002, 2004, 2008). Hubert et al. (2005) showed statistically that the characteristic decay time of such arcs is ~199 s on average, with a standard deviation of ~132 s. The estimated lifetime of less than 6 min of the observed detached auroras is therefore comparable with the known properties of these dayside arcs (also known as dayside subauroral proton flashes).

3.2. NOAA Observations of the Detached Aurora

During the event five POES satellites were in operations POES 15, 16, 17, 18, and 19. When the pressure enhancement hit the Earth they were all in different positions around the Earth, some in the auroral zone and some at other locations. Only POES 19 could detect the detached arc.

At ~11:06 UT, 2 min after the pressure enhancement hit the Earth, the NOAA 19/POES flew across and monitored the southern auroral oval around 1300 MLT. Its conjugate position is in the latitudes of the northern detached arc, which was noted by a triangle in Figure 3b. Figure 6 presents the proton and electron observations from NOAA 19. In Figure 6a, it is clearly seen that there were two strong proton peaks. One peak was around 67° MLAT (to the left of the green dashed box) representing the auroral oval. Another strong proton precipitation (inside the green box) was located at ~62° MLAT and separated from the main auroral oval. This

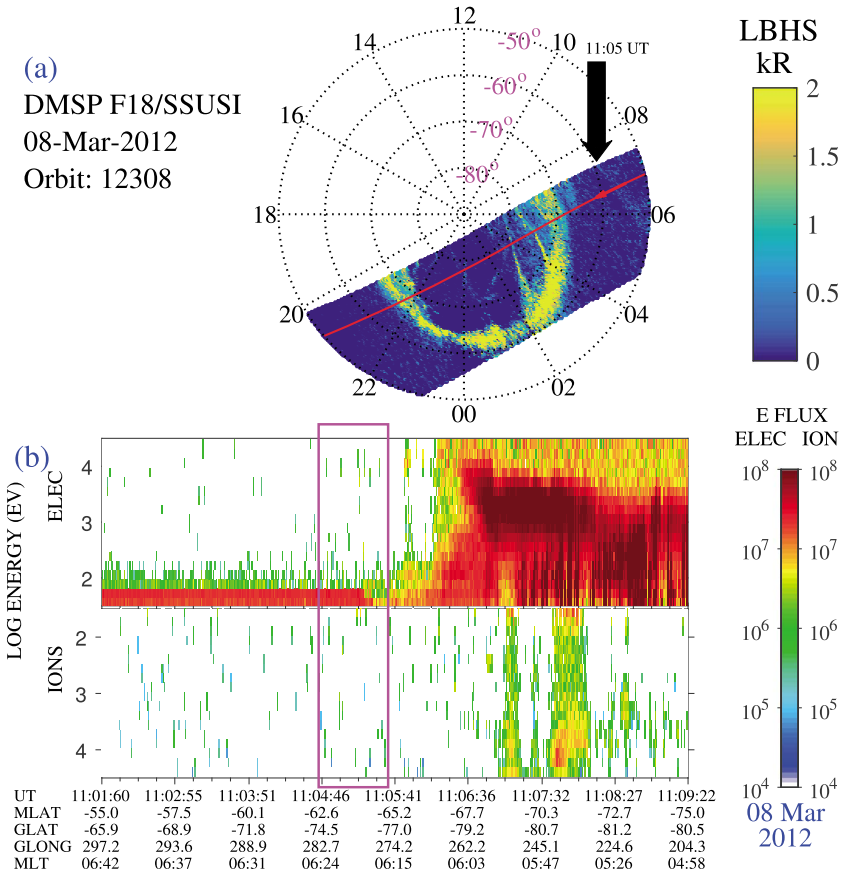

Figure 5. (a) Southern auroral Lyman-Birge-Hopfield Short (LBHS) image obtained by the Defense Meteorological Satellite Program (DMSP) F18/SSUSI on 8 March 2012, similar to Figure 1. (b) The differential energy flux for precipitating electrons and ions. The conjugate ionospheric footprint, as directed by a black arrow in panel (a) and a box in panel (b), of the northern detached aurora was crossed by DMSP F18 at 11:05 UT, nearly the same time as the northern detached aurora (11:06 UT). On can see there is no detached aurora in the southern dawn sector. SSUSI = Special Sensor Ultraviolet Spectrographic Imager; MLAT = magnetic latitude; MLT = magnetic local time.

detached proton aurora peaked around 62° MLAT at ~11:06 UT. It was in the same magnetic latitudes and occurred at the same time as the dawnside detached arc in Northern Hemisphere (Figure 3b). Thus, it was most probably be a part of a dayside detached arc conjugate to the northern one. It is reasonable to assume that the detached arcs were conjugate and both arcs could extend to 1300 MLT at least. In Figure 6a, both the 30–80 keV and 80–240 keV proton precipitations increased at the detached aurora location. Figure 6b gives low-energy protons in the 0° telescope of TED. However, they show no increase in the arc position. Also, around 62° MLAT there was no clear enhancement in the energy input of low energy protons (Figure 6c). Figure 6d gives the energy for maximum proton auroral flux in the energy range 0.1–20 keV. This energy was above 10 keV in the arc region (between the green lines), similar to the energy spectrum of the dayside detached arc (Figure 4, lower panel). Figures 6e–6h gives the electron observations. Looking at Figure 6e the electrons above 30 keV go down in the detached auroral region except for the small spike around 11:06:30 UT. Even so, the detached aurora should be dominated by high energy protons rather than electrons, as the detached aurora was located in a wider MLAT ranging from 60° to 65°. In a word, the detached aurora from NOAA POES 19 observation has many similarities with the northern dawnside detached arc (Figures 3 and 4). They occurred at similar latitudes and at the same time, that is, 11:06 UT, 2 min after the pressure enhancement, and are both associated with proton precipitations only. These suggest the detached auroras were conjugate and the corresponding energetic particles came from the same source region. Note that for the protons inside the northern detached arc, the DMSP F16 showed more ion precipitations above 20 keV but cannot detect particles above 30 keV. NOAA observations further indicated that the detached auroras were contributed by energetic protons

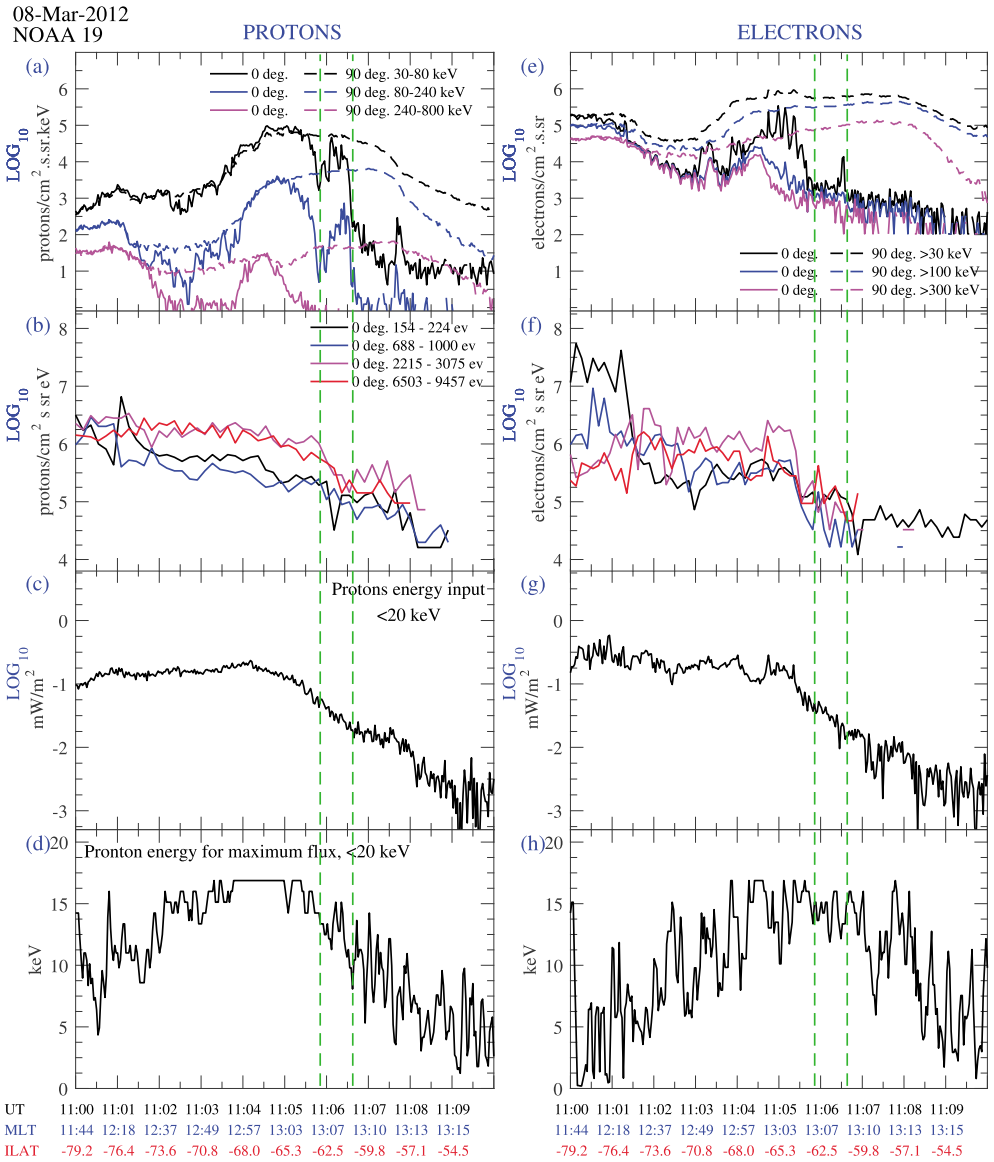

Figure 6. Protons and electrons observations from National Oceanic and Atmospheric Administration (NOAA) 19/POES Medium Energy Proton and Electron Detector (MEPED) and Total Energy Detector (TED) instruments on 8 March 2012. (a) MEPED proton differential energy flux in the 0° and 90° telescopes in three energy bands, 30–80 keV, 80–240 keV and 240–800 keV. (b) TED protons from the 0° telescope in four energy bands, 154–224 eV, 688–1000 eV, 2215–3075 eV and 6503–9457 eV. (c) Integrated omnidirectional energy flux deposited in the ionosphere through a surface perpendicular to the magnetic field based on proton measurements in the energy range of 0.1–20 keV. (d) Center energy for the proton energy band where the maximum directional energy flux in the energy range 0.1–20 keV is measured. (e–h) Similar to the corresponding left-hand panels but for electrons. At the bottom of the plots, the UT, magnetic local time (MLT) and magnetic latitude (MLAT) are given. The green dotted lines note the position between 61° and 63° MLAT.

above 30 keV, extending up to more than 80 keV, undoubtedly from the ring current. In addition, for the detached aurora shown in Figure 6a, the proton flux in the 90° telescope is higher than in the 0° telescope, giving an anisotropic pitch angle distribution, in contrast with the isotropic precipitations in the auroral oval (Sergeev et al., 1983).

4. Discussion

In the present study the DMSP F16/SSUSI and NOAA 19/POES both observed a detached aurora equatorward of the auroral oval. They were observed at around 11:06 UT on 8 March 2012, just 2 min after the sudden solar

wind pressure ramp hit the Earth (11:04 UT). These detached auroras were most probably conjugate and had a short duration less than 6 min, coincident with the impact of pressure enhancement. These characteristics are similar as the shock-induced detached auroras reported by previous studies (Fuselier et al., 2004; Hubert et al., 2003; Zhang et al., 2002, 2008). Zhang et al. (2002) reported that the dayside detached auroras were contributed by protons with energies on the order of ~10 keV, but there can also be an important case to case variability. The previous DMSP observation was not satisfied for proton auroras with high energy, since it cannot detect particles above 30 keV. In the present work, DMSP and NOAA in situ particle observations were combined. Our observations show that the energetic protons above 20 keV were predominant in the detached auroras and their particle energy reached up to a few hundreds of keV, without significant electron precipitations. The present detached arc occurred during the recovery of a −92 nT storm when the ring current was filled with hot ions/protons. We suggest that these energetic protons from the ring current caused the detached arc. The high energy of these particles could explain why the LBHS emitted by the detached arc is weaker than the LBHL emission (Figure 3). The reason is that the energetic protons can precipitate into lower altitude, where the oxygen is abundant, and the LBHS instead of LBHL is absorbed effectively by molecular oxygen (O_2) (Germany et al., 1997). It is worth noting that the absorption of LBH emission produced by the protons depends weakly on the proton energy (Hubert et al., 2001).

The precipitation mechanism of energetic protons could be related to the change of the loss cone. Particles that mirror below about 150 km can easily collide with the dense atmosphere and be lost, producing auroral emissions (Störmer, 1946). The pitch angle corresponding to magnetic mirror around 150 km is the critical pitch angle, and all particles with pitch angles less than this will be lost into the atmosphere. Note that the altitude where the particles are lost depends on the particle energies (Turunen et al., 2009). The size of the loss cone can be expressed as $\sin^2\alpha = B_e/B_m$, where α is the critical pitch angle, B_e and B_m refer to the magnetic fields at equatorial plane in the magnetosphere and mirroring point in the ionosphere, respectively. When the magnetosphere is compressed by the increasing solar wind pressure, both the B_e and B_m will increase suddenly. However, the magnetic field intensity in equatorial plane (B_e) is much weaker than at magnetic mirror (B_m), and B_e is hit by the enhanced pressure first; thus, it is expected that the B_e will relatively increase much more than B_m. It turns out that an increase of B_e enlarges the loss cone, so that more particles can reach denser layers of the ionosphere, precipitating into the atmosphere. Figure 7a shows the total magnetic field intensity measured by the GOES-13 satellite at L = 6.6. The GOES-13 moved over 0600 MLT, which basically agreed with the location of the detached arc (Figure 3b). Figure 7a exhibits the variations of the total magnetic field strength caused by the solar wind pressure enhancement. The magnetic field intensity at GOES (L = 6.6) increased from 120 nT to 152 nT. The arc was observed at 63° MLAT. The terrestrial magnetic field is reasonably assumed to be a dipole field for L shell less than 5. Using the formula $L = 1/(\cos(\mathrm{MLAT}))^2$ introduced by Kivelson and Russell (1995), we estimate that the detached arc is mapped to L = 4.9 in the equatorial plane. As the GOES was close to L = 4.9, it is reasonable to assume that the magnetic intensity at L = 4.9 increased similarly to the magnetic intensity measured by the GOES-13, that is, by 26.6% increase. The total magnetic field in the arc location is ~52,000 nT (from International Geomagnetic Reference Field model) at the ionospheric altitude; thus, the loss cone was respectively 4.30° and 4.85° before and after the pressure enhancement. Thus, the loss cone increased by 13%.

Now, we consider 50 keV protons and assume that they are located at L = 5 in the equatorial plane. The bounce period is estimated to be 42 s for these protons (Baumjohann & Treumann, 2012). In the present case, the solar wind pressure pulse between ~11:05 and ~11:06 UT would contribute to the formation of the detached arc. The solar wind pressure pulse increased from 12 to 30 nP during 15 s. It is expected that this small time scale of the pressure increase, during which B_e changes, is shorter than the proton bounce period, so that the high energy protons have not enough time to adapt to the magnetic field change, and the second adiabatic invariant will be violated. Thus, the loss cone of the protons can be expected to increase significantly and much more protons will get lost into the ionosphere. In addition to the pressure pulse mentioned here, the persisted solar wind pressure enhancement could cause the proton aurora, as have been reported in previous investigations (Laundal & Østgaard, 2008; Liou et al., 2007).

Previous studies suggested that the EMIC wave could be responsible for the detached proton arc caused by pressure pulse (Fuselier et al., 2004; Hubert et al., 2003, 2005; Yahnina et al., 2008; Zhang et al., 2002, 2008; Zhou & Tsurutani, 1999). The magnetic field intensity at equatorial plane is reasonably assumed to increase

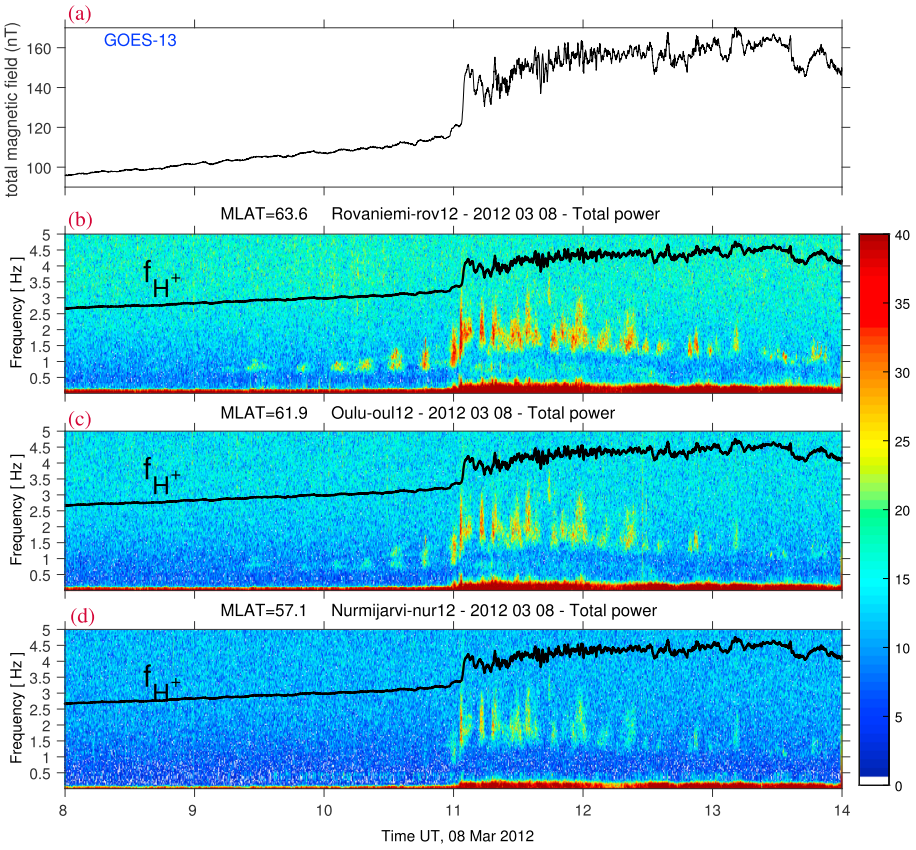

Figure 7. (a) The total magnetic field at the equatorial plane, using data from GOES-13, a geosychronous satellite. (b–d) Spectrograms of the horizontal components of Pc1 pulsations from Rovaniemi (magnetic latitude (MLAT) = 63.6°, L = 5.1), Oulu (MLAT = 61.9°, L = 4.6), and Nurmijärvi (MLAT = 57.1°, L = 3.4) stations between 08 and 14 UT on 8 March 2012. The color maps in panels b–d are in dB scale. At around 11:00 UT, the three stations were located between 1300 and 1400 magnetic local time. Panels (b), (c) and (d) give the proton gyrofrequency at magnetic equatorial plane corresponding to the dawnside detached arc.

when the magnetosphere is compressed by the solar wind pressure enhancement, as seen from Figure 7a. As the first adiabatic invariant and the total energy are conserved, the temperature anisotropy can be expected to increase after the magnetosphere compressed by the solar wind dynamic pressure enhancement, resulting in the ion cyclotron instability (Anderson & Hamilton, 1993; Liu et al., 2017; Zhou & Tsurutani, 1999). At the same time the enhanced pressure can be expected to compress the ring current, bringing it closer to the Earth (Wang et al., 2003), encountering with the cold and dense plasmasphere which lowers the instability threshold (Gary et al., 1995). As a result, EMIC waves may be easily generated and amplified, scattering the energetic ions into the loss cone (Anderson & Hamilton, 1993; Fuselier et al., 2004; Gary et al., 1995; Søraas & Aarsnes, 1996).

When the detached auroras occurred the EMIC wave activity as well increased. Figures 7b–7d show the EMIC waves on 8 March 2012 from three Finnish pulsation magnetometers: Rovaniemi (MLAT = 63.6), Oulu (MLAT = 61.9), and Nurmijärvi (MLAT = 57.1). When the pressure enhancement hit the Earth, these ground stations were located in the afternoon sector, between 1300 and 1400 MLT, which was near the conjugate position of the southern proton precipitations observed by NOAA 19 (Figure 6). All these stations showed intense EMIC waves between 0 and 4 Hz after about 11:00 UT, in line with the occurrence time of the pressure enhancement and the detached arc. In Figure 7, we can see several EMIC enhancements between 11:00 and 12:00 UT, but each of them only persisted for a few minutes. There seems to be a good coincidence between these pulsed EMIC waves measured by ground stations in Finland, and the pulsed solar wind pressures between 11:00 and 12:00 UT (Figure 1). It is seen that the total magnetic field strength increased with time, which is expected to cause an adiabatically energization of the protons preferentially in the direction normal

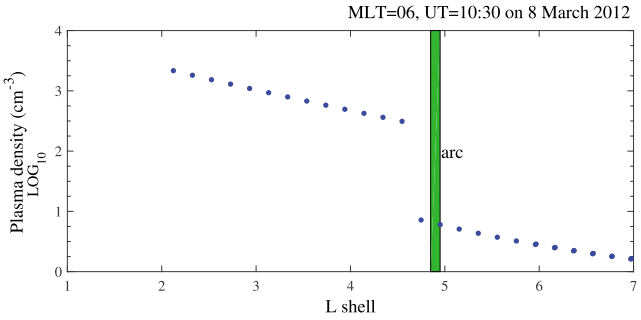

Figure 8. The modeled plasma density in the equatorial plane for the dawnside arc region. The green area denotes the L shell 4.9, where the detached arc is mapped. See the text for more details about getting the L value corespoding to the detached arc. MLT = magnetic local time.

to the magnetic field, increasing their anisotropy probably and making them unstable and likely to generate EMIC waves (Anderson & Hamilton, 1993; Zhou & Tsurutani, 1999). It is also seen that the frequency of the EMIC waves increased with time, in agreement with the magnetic strength (Figure 7a), suggesting that the EMIC waves are expected to be modulated by the magnetic field.

Erlandson et al. (1996) observed the EMIC waves inside the plasmapause. Yahnin et al. (2013) found that most subauroral proton spot sources were located in the vicinity of the plasmapause or inside the plasmapause. In the present investigation, we ran a three-dimensional dynamic kinetic model of the plasmasphere (Pierrard & Stegen, 2008) to study the relationship of plasmapause and detached aurora. This model takes into account the rotation of the plasmasphere as well as the geomagnetic activity that determines the position and width of the plasmapause region. The Kp-dependent empirical electric field model E5D is included in this plasmasphere model. In previous studies, this plasmasphere model reproduced the plasmapause in agreement with the observations of Imager for Magnetopause-to-Aurora Global Exploration (IMAGE) (Pierrard & Stegen, 2008). Figure 8 shows the modeling plasmasphere density at the 0600 MLT sector, where the northern detached arc was observed. The L shell value of the detached arc is also marked, showing that the particles producing the detached aurora were originated from the vicinity of the plasmapause. This location of the source region of the present detached aurora is in general consistent with the results of previous investigations. The solar wind pressure enhancement struck the magnetosphere and would probably increase the transverse anisotropy of the proton temperature, which was a primary source for the ion cyclotron instability. In addition, as shown in Figure 8, the cold plasma density and its density gradient in the plasmapause are also important parameters for the growth of the EMIC waves (Cornwall et al., 1970; Kozyra et al., 1984). Cold plasma density gradients are expected to enable the instability growth rate to be maximized (Cornwall et al., 1970; Horne & Thorne, 1993). The detached arc occurred during the recovery phase of a moderate storm with the minimum SMR of −90 nT. Consequently, the ring current was reasonably assumed to containe a fair amount of energetic ions/protons, which had enough energy to resonate with the EMIC waves. The hot protons would give energy to EMIC waves and were scattered into the loss cone likely producing the detached auroras. The lower limit resonance energy E_R can be expressed (Kennel & Petschek, 1966) as

$$E_R = \frac{B^2}{2\mu_0 N}\left(\frac{\omega_c^+}{\omega}\right)^2\left(1-\frac{\omega}{\omega_c^+}\right)^3$$

Here B is the ambient magnetic field and its value is 371 nT as mentioned above. μ_0 is vacuum permeability, $4\pi \times 10^{-7}$ Tm/A. N is the plasma number density, which is estimated to be 6 per cubic centimeter at $L = 4.9$ for the arc (Figure 8). ω_c^+ is proton gyrofrequency. ω is the EMIC wave frequency which is estimated to be 3 Hz after the pressure enhancement (Figure 7). Therefore, the resonance energy is about 21 keV, which means that the protons with energy above 21 keV can resonate with the EMIC waves. This result is consistent with the in situ observations from DMSP and NOAA satellites.

In Figure 6b, the low-energy protons decreased in the detached auroral region from TED observation. The low-energy protons could not resonate with EMIC waves, and they are subjected to weak pitch angle scattering (slow pitch angle diffusion) as described by Kennel and Petschek (1966). That means the proton flux decreases from the edge of the loss cone to the center. This flux might be underestimated, which were associated with the loss cone change. The loss cone increased rapidly during the events; thus, the relative distance between the detector and the loss cone center became nearer, which will lead to possible underestimation for a limited view field of the detector.

Laundal and Østgaard (2008) displayed the proton aurora caused by the solar wind pressure enhancement, while their study focused on the main auroral oval. Søraas et al. (2013) showed a prolonged detached arc produced by energetic protons. That arc was found in the postmidnight and lasted for 2 hr. Its lasting time was consistent with the gradually increased solar wind pressure. But the detached auroras in this work were caused by the solar wind pressure enhancement and persisted for less than 6 min. We found a consistent association between the observed pressure enhancement, detached arc, and EMIC waves. The northern

detached arc was observed at the dawnside and probably extended to the afternoon sector, which was in a conjugate latitudes of the southern detached proton aurora observed at the same time (11:06 UT) by NOAA 19/POES. Thus, the detached aurora in the present work was most likely a conjugate phenomenon.

5. Summary and Conclusions

A transient detached aurora event was detected on 8 March 2012 around 11:06 UT by the DMSP F16/SSUSI, SSJ, and NOAA 19/POES through imaging and in situ observations. This event occurred 2 min after a sudden solar wind pressure ramp struck the magnetosphere at 11:04 UT, with a detached ion aurora in each hemisphere. The detached auroras occurred during the recovery phase of a moderate storm and were produced by unusually high-energy ions. Some detailed characteristics of these detached auroras are summarized as follows:

1. A detached auroral arc was observed by DMSP 16/SSUSI at 11:06 UT in the Northern Hemisphere. It was located from 0530 MLT to 0830 MLT with possible further MLT extension, and between 60° and 65° MLAT. Its location was separated by about 5° MLAT from the equatorward edge of the main auroral oval. At the same time, NOAA 19 POES measured a similar detached aurora in the southern hemisphere, centered around 62° MLAT and 1300 MLT and seperated from the auroral oval.
2. Particle observations revealed that both detached auroras were produced by proton/ion precipitations without evident electron contribution. They were dominated by energetic protons from ~20 keV to more than 80 keV, much higher than the ~10 keV suggested by previous studies.
3. These detached auroras were associated with the dynamic pressure ramp that hit the Earth's magnetosphere at ~11:04 UT. They had short duration less than 6 min, coincident with the impact of the pressure pulse and comparable with the known average characteristic lifetime of these dayside detached auroras. They also took place during the recovery of a moderate storm having a minimum SMR of −90 nT. Thus, the ring current can reasonably be assumed to have a large number of hot ions/protons acting as source for the detached arc.
4. We estimate that the solar wind dynamic pressure enhancement increased the magnetic field strength in the equatorial plane much more than at low altitude, increasing the loss cone size by 13%.
5. Our physical understanding of the observation is that the solar wind pressure enhancement compressed the magnetosphere, increased the temperature anisotropy of the protons, and pushed the protons close to the plasmapause where the steep gradient of cold plasma favored the EMIC wave growth. The hot protons resonated with EMIC waves, providing them energy, and were scattered into the loss cone producing the detached proton auroras.

The above results show that there is a close association between the detached auroras, plasmapause plasma density variation, pressure enhancement, and enhancement of the EMIC wave. It is highly likely that the pressure enhancement, the density variation, and the change in the loss cone initiated the conditions for wave growth and the precipitation of the higher-energy protons giving rise to the detached aurora.

Acknowledgments
We acknowledge Johns Hopkins University Applied Physics Laboratory for providing the DMSP/SSUSI, SSJ in situ data and SuperMag Ring Current indices (SMR). The SSUSI data are available from https://ssusi.jhuapl.edu/. The DMSP particle data can be download from http://sd-www.jhuapl.edu/Aurora/. The SMR indices are download from http://supermag.jhuapl.edu/. The authors thank the Sodankylä Geophysical Observatory operating the magnetometers and providing the geomagnetic pulsation data (http://www.sgo.fi/Data/ Pulsation/). The authors as well thank NOAA for supporting the POES program. We thank Hilde Nesse Tyssøy, in Birkeland Centre for Space Science (BCSS), for providing the calibrated NOAA POES data and Marit Sandanger (BCSS) for calculating the change in the particle loss cone distribution. We would like to acknowledge Cluster CIS and FGM instrument teams. The Cluster data were available from the Cluster Science Archive (https://www.cosmos.esa.int/web/csa/access). We would like to thank Viviane Pierrard and Kris Borremans from Belgian Institute for Space Aeronomy for giving the modeled plasmasphere density data. This study was supported by the Research Council of Norway under contract 223252/F50 (CoE), National Natural Science Foundation of China (41674154, 41421063, and 41325017), the Project of Chinese Academy of Sciences (KZZD-EW-01) of the Chinese Academy of Sciences, and the Fundamental Research Funds for the Central Universities (WK2080000077).

References

Anderson, B. J., & Hamilton, D. C. (1993). Electromagnetic ion cyclotron waves stimulated by modest magnetospheric compressions. *Journal of Geophysical Research*, *98*(A7), 11,369–11,382. https://doi.org/10.1029/93JA00605

Anger, C. D., Moshupi, M. C., Wallis, D. D., Murphree, J. S., Brace, L. H., & Shepherd, G. G. (1978). Detached auroral arcs in the trough region. *Journal of Geophysical Research*, *83*(A6), 2683–2689. https://doi.org/10.1029/JA083IA06P02683

Baumjohann, W., & Treumann, R. A. (2012). *Basic space plasma physics*. London: Imperial College Press. https://doi.org/10.1142/p850

Burch, J. L., Lewis, W. S., Immel, T. J., Anderson, P. C., Frey, H. U., Fuselier, S. A., et al. (2002). Interplanetary magnetic field control of afternoon-sector detached proton auroral arcs. *Journal of Geophysical Research*, *107*(A9), 1251. https://doi.org/10.1029/2001JA007554

Cornwall, J. M., Coroniti, F. V., & Thorne, R. M. (1970). Turbulent loss of ring current protons. *Journal of Geophysical Research*, *75*, 4699–4709. https://doi.org/10.1029/JA075I025p04699

Erlandson, R. E., Mursula, K., & Bösinger, T. (1996). Simultaneous ground-satellite observations of structured Pc 1 pulsations. *Journal of Geophysical Research*, *101*(A12), 27,149–27,156. https://doi.org/10.1029/96JA02645

Evans, D. S., & Greer, M. S. (2000). Polar orbiting environmental satellite space environment monitor—2: Instrument description and archive data documentation, NOAA Technical Memorandum OAR SEC (93 pp.). Boulder, CO: National Oceanic and Atmospheric Administration.

Frey, H. U. (2007). Localized aurora beyond the auroral oval. *Reviews of Geophysics*, *45*, RG1003. https://doi.org/10.1029/2005RG000174

Fuselier, S. A., Gary, S. P., Thomsen, M. F., Claflin, E. S., Hubert, B., Sandel, B. R., & Immel, T. (2004). Generation of transient dayside subauroral proton precipitation. *Journal of Geophysical Research*, *109*, A12227. https://doi.org/10.1029/2004JA010393

Gary, S. P., Thomsen, M. F., Yin, L., & Winske, D. (1995). Electromagnetic proton cyclotron instability: Interactions with magnetospheric protons. *Journal of Geophysical Research*, *100*, 21,961–21,972. https://doi.org/10.1029/95JA01403

Germany, G. A., Parks, G. K., Brittnacher, M., Cumnock, J., Lummerzheim, D., Spann, J. F., et al. (1997). Remote determination of auroral energy characteristics during substorm activity. *Geophysical Research Letters*, *24*, 995–998. https://doi.org/10.1029/97GL00864

Germany, G. A., Torr, M. R., Richards, P. G., & Torr, D. G. (1990). The dependence of modeled OI 1356 and N_2 Lyman Birge Hopfield auroral emissions on the neutral atmosphere. *Journal of Geophysical Research*, *95*(A6), 7725–7733. https://doi.org/10.1029/JA095IA06P07725

Horne, R. B., & Thorne, R. M. (1993). On the preferred source location for the convective amplification of ion cyclotron waves. *Journal of Geophysical Research*, *98*(A6), 9233–9247. https://doi.org/10.1029/92JA02972

Hubert, B., Gérard, J.-C., Bisikalo, D. V., Shematovich, V. I., & Solomon, S. C. (2001). The role of proton precipitation in the excitation of auroral FUV emissions. *Journal of Geophysical Research*, *106*(A10), 21,475–21,494. https://doi.org/10.1029/2000JA000288

Hubert, B., Gérard, J. C., Fuselier, S. A., & Mende, S. B. (2003). Observation of dayside subauroral proton flashes with the IMAGE-FUV imagers. *Geophysical Research Letters*, *30*(3), 1145. https://doi.org/10.1029/2002GL016464

Hubert, B., Gérard, J. C., Mende S. B., & Fuselier S. A. (2005). Statistical properties of dayside subauroral proton flashes observed with IMAGE-FUV. In J. L. Burch, M. Schulz, & H. Spence (Eds.), *Inner Magnetosphere Interactions: New Perspectives from Imaging*, *AGU Geophysical Monograph Series* (Vol. 159, pp. 195–205). Washington, DC: American Geophysical Union. https://doi.org/10.1029/159GM15

Immel, T. J., Mende, S. B., Frey, H. U., Peticolas, L. M., Carlson, C. W., Gérard, J.-C., et al. (2002). Precipitation of auroral protons in detached arcs. *Geophysical Research Letters*, *29*(11), 1519. https://doi.org/10.1029/2001GL013847

Kennel, C. F., & Petschek, H. E. (1966). Limit on stably trapped particle fluxes. *Journal of Geophysical Research*, *71*, 1–28. https://doi.org/10.1029/JZ071I001P00001

Kivelson, M. G., & Russell, C. T. (1995). *Introduction to space physics* (166 pp.). Cambridge: Cambridge University Press.

Kozyra, J. U., Cravens, T. E., Nagy, A. F., Fontheim, E. G., & Ong, R. S. B. (1984). Effects of energetic heavy ions on electromagnetic ion cyclotron wave generation in the plasmapause region. *Journal of Geophysical Research*, *89*(A4), 2217–2233. https://doi.org/10.1029/JA089IA04P02217

Laundal, K. M., & Østgaard, N. (2008). Persistent global proton aurora caused by high solar wind dynamic pressure. *Journal of Geophysical Research*, *113*, A08231. https://doi.org/10.1029/2008JA013147

Liou, K., Newell, P. T., Shue, J.-H., Meng, C.-I., Miyashita, Y., Kojima, H., & Matsumoto, H. (2007). "Compression aurora": Particle precipitation driven by long-duration high solar wind ram pressure. *Journal of Geophysical Research*, *112*, A11216. https://doi.org/10.1029/2007JA012443

Liu, Y., Lei, J., Yu, P., Zhang, Z., Zhang, X., & Cao, J. (2017). Laboratory generation of broadband ELF waves by inhomogeneous plasma flow. *Geophysical Research Letters*, *44*, 1634–1640. https://doi.org/10.1002/2016GL072232

Moshupi, M. C., Cogger, L. L., Wallis, D. D., Murphree, J. S., & Anger, C. D. (1977). Auroral patches in the vicinity of the plasmapause. *Geophysical Research Letters*, *4*, 37–40. https://doi.org/10.1029/GL004I001P00037

Newell, P. T. (2000). Reconsidering the inverted-V particle signature: Relative frequency of large-scale electron acceleration events. *Journal of Geophysical Research*, *105*, 15,779–15,794. https://doi.org/10.1029/1999JA000051

Paxton, L. J., Morrison, D., Zhang, Y., Kil, H., Wolven, B., Ogorzalek, B. S., et al. (2002). Validation of remote sensing products produced by the Special Sensor Ultraviolet Scanning Imager (SSUSI): A far UV-imaging spectrograph on DMSP F-16.

Pierrard, V., & Stegen, K. (2008). A three-dimensional dynamic kinetic model of the plasmasphere. *Journal of Geophysical Research*, *113*, A10209. https://doi.org/10.1029/2008JA013060

Sandanger, M. I., Ødegaard, L.-K. G., Nesse Tyssøy, H., Stadsnes, J., Søraas, F., Oksavik, K., & Aarsnes, K. (2015). In-flight calibration of NOAA POES proton detectors—Derivation of the MEPED correction factors. *Journal of Geophysical Research: Space Physics*, *120*, 9578–9593. https://doi.org/10.1002/2015JA021388

Sergeev, V. A., Sazhina, E. M., Tsyganenko, N. A., Lundblad, J. Å., & Søraas, F. (1983). Pitch-angle scattering of energetic protons in the magnetotail current sheet as the dominant source of their isotropic precipitation into the nightside ionosphere, *Planetary and Space Science*, *31*(10), 1147–1155. https://doi.org/10.1016/0032-0633(83)90103-4

Shue, J.-H., Chao, J. K., Fu, H. C., Russell, C. T., Song, P., Khurana, K. K., & Singer, H. J. (1997). A new functional form to study the solar wind control of the magnetopause size and shape. *Journal of Geophysical Research*, *102*(A5), 9497–9511. https://doi.org/10.1029/97JA00196

Søraas, F., & Aarsnes, K. (1996). Observations of ENA in and near a proton arc. *Geophysical Research Letters*, *23*, 2959–2962. https://doi.org/10.1029/96GL02821

Søraas, F., Laundal, K. M., & Usanova, M. (2013). Coincident particle and optical observations of nightside subauroral proton precipitation. *Journal of Geophysical Research: Space Physics*, *118*, 1112–1122. https://doi.org/10.1002/JGRA.50172

Sotirelis, T., Korth, H., Hsieh, S.-Y., Zhang, Y., Morrison, D., & Paxton, L. (2013). Empirical relationship between electron precipitation and far-ultraviolet auroral emissions from DMSP observations. *Journal of Geophysical Research: Space Physics*, *118*, 1203–1209. https://doi.org/10.1002/JGRA.50157

Störmer, C. (1946). Frequency of 12,330 measured heights of aurora from southern Norway in the years 1911–1944. *Terrestrial Magnetism and Atmospheric Electricity*, *51*(4), 501–504. https://doi.org/10.1029/TE051I004P00501

Turunen, E., Verronen, P. T., Seppälä, A., Rodger, C. J., Clilverd, M. A., Tamminen, J., et al. (2009). Impact of different energies of precipitating particles on NO_x generation in the middle and upper atmosphere during geomagnetic storms. *Journal of Atmospheric and Terrestrial Physics*, *71*(10–11), 1176–1189. https://doi.org/10.1016/J.JASTP.2008.07.005

Usanova, M. E., Mann, I. R., Kale, Z. C., Rae, I. J., Sydora, R. D., Sandanger, M., et al. (2010). Conjugate ground and multisatellite observations of compression-related EMIC Pc1 waves and associated proton precipitation. *Journal of Geophysical Research*, *115*, A07208. https://doi.org/10.1029/2009JA014935

Wang, C. B., Chao, J. K., & Lin, C. H. (2003). Influence of the solar wind dynamic pressure on the decay and injection of the ring current. *Journal of Geophysical Research*, *108*(A9), 1341. https://doi.org/10.1029/2003JA009851

Yahnin, A. G., Yahnina, T. A., Frey, H., & Pierrard, V. (2013). Sub-oval proton aurora spots: Mapping relatively to the plasmapause. *Journal of Atmospheric and Terrestrial Physics*, *99*, 61–66. https://doi.org/10.1016/J.JASTP.2012.09.018

Yahnina, T. A., Frey, H. U., Bösinger, T., & Yahnin, A. G. (2008). Evidence for subauroral proton flashes on the dayside as the result of the ion cyclotron interaction. *Journal of Geophysical Research*, *113*, A07209. https://doi.org/10.1029/2008JA013099

Zhang, Y., Paxton, L. J., Immel, T. J., Frey, H. U., & Mende, S. B. (2002). Sudden solar wind dynamic pressure enhancements and dayside detached auroras: IMAGE and DMSP observations. *Journal of Geophysical Research*, *108*(A4), 8001. https://doi.org/10.1029/2002JA009355

Zhang, Y., Paxton, L. J., Meng, C. I., Morrison, D., Wolven, B., Kil, H., & Christensen, A. B. (2004). Double dayside detached auroras: TIMED/GUVI observations. *Geophysical Research Letters*, *31*, L10801. https://doi.org/10.1029/2003GL018949

Zhang, Y., Paxton, L. J., & Zheng, Y. (2008). Interplanetary shock induced ring current auroras. *Journal of Geophysical Research*, *113*, A01212. https://doi.org/10.1029/2007JA012554

Zhou, X., & Tsurutani, B. T. (1999). Rapid intensification and propagation of the dayside aurora: Large scale interplanetary pressure pulses (fast shocks). *Geophysical Research Letters*, *26*, 1097–1100. https://doi.org/10.1029/1999GL900173